Measurement of the proton-carbon bremsstrahlung cross sections at 2.135 MeV: Testing soft-photon approximations

D. Yan, P. M. S. Lesser, M. K. Liou, and C. C. Trail
Department of Physics and Institute for Nuclear Theory, Brooklyn College of the City University of New York, Brooklyn, New York 11210
(Received 10 June 1991)

The proton-carbon bremsstrahlung ($p\,^{12}C\gamma$) cross sections as a function of photon energy have been measured at the incident proton energy of 2.135 MeV for two proton scattering angles: one at 155° and another one at 175°. We have extended the range of photon energy up to about 1.7 MeV, which is near the maximum photon energy, in order to study all possible resonant structures. Two resonant structures have been observed in the bremsstrahlung spectrum. The first is identified as the structure due to the 1.7-MeV elastic $p\,^{12}C$ scattering resonance and the second is attributed to the 0.5-MeV resonance. These measured $p\,^{12}C\gamma$ spectra with the detailed information about the resonant structure have been used to test the range of validity of various soft-photon approximations. We have found that our data can be described by a special two-energy–two-angle approximation, which depends on one elastic T matrix evaluated at the initial energy (or total energy squared) and another elastic T matrix evaluated at the final energy, but the approximation is free of any derivative of the elastic T matrix with respect to energy or scattering angle (or momentum transfer squared). Our study also shows that the resonant structure predicted by the one-energy–one-angle approximation disagrees with the experimental data.

PACS number(s): 25.40.−h, 12.20.Fv, 13.40.−f

I. INTRODUCTION

It was pointed out in a previous paper [1] that precise measurements of the proton-carbon bremmstrahlung ($p\,^{12}C\gamma$) cross sections with all information about any resonances present, their position in the photon energy spectrum and their width, can provide a very sensitive test of various soft-photon approximations. In this paper, we wish to report measurements at the incident proton energy of 2.135 MeV for two scattering angles and to show that our data can indeed be used to differentiate among various soft-photon approximations.

The $p\,^{12}C\gamma$ process has been studied with great interest both experimentally [2–5] and theoretically [1,6–9] during the past fifteen years. In addition to the investigation of the off-shell effects, the other reasons for studying this process can be summarized as follows: (i) to measure the $p\,^{12}C\gamma$ cross sections as a function of photon energy near an elastic $p\,^{12}C$ scattering resonance and to verify experimentally the existence of the resonant structure in the bremsstrahlung spectrum, (ii) to study the range of validity of Low's original soft-photon approximation [10] and the Feshbach-Yennie approximation [6,11] and to see if these approximations can be used to describe the $p\,^{12}C\gamma$ cross sections in the energy region of a resonance, and (iii) to extract from the data the nuclear time delay which can be used to distinguish unambiguously between direct nuclear reactions and compound nuclear reactions. The combined experimental and theoretical studies turn out to be very successful, not only that the resonant structures near both the 1.7-MeV and the 0.5-MeV elastic scattering resonances have been observed but also that a delay time of order of 10^{-20} second has been extracted from the experimental data. However, all experiments performed in the past measured the $p\,^{12}C\gamma$ cross sections only in the soft-photon region since the bombarding energies used in these experiments were just slightly above the resonance energy. No effort has been made to extend the range of measurement up to the hard-photon region (or up to the maximum photon energy) so that all possible resonant structures can be studied. Measurement of all possible resonant structures in the whole bremsstrahlung spectrum has become an important experimental work because, as pointed out in Ref. [1], the result of such a measurement can be used to test the validity of various theoretical approximations and models. We consider the low-energy $p\,^{12}C\gamma$ process an ideal process for testing soft-photon approximations since all complications due to the spin and magnetic moment of the proton and the intermediate particle $^{13}N^*$ can be completely ignored. These complications are irrelevant to the testing of various soft-photon approximations.

II. EXPERIMENTAL METHODS

The experimental arrangement basically follows our earlier setup for the $p\,^{12}C\gamma$ and $p\,^{16}O\gamma$ measurements [3,5,12]. We detect the coincident events between scattered protons and photons emitted perpendicular to the scattering plane. Protons of 2.135 MeV from the Brooklyn College 3.75-MV Dynamitron Accelerator are incident upon a 50-$\mu g/cm^2$-thick carbon foil, which is tilted 45° with respect to the incident beam. The beam, about 600 nA, is about 2 mm in diameter. Scattered protons are detected by two silicon surface barrier detectors. An annular detector subtends a solid angle of 3 msr and

has an average scattering angle of about 175°. A second detector at 155° subtends 2 msr. Gamma rays emitted perpendicular to the scattering plane are detected by a 76 mm × 76 mm NaI (Tl) detector located 22 mm above the scattering plane. Standard fast-slow coincidence circuitry is used to give an event mode listing of the data which is stored in an IBM PC computer for off-line analysis. The fast-timing resolution of about 4 ns (FWHM), and kinematic constraints placed on the data reduce background events to about 3% of the data.

A two-dimensional plot of coincidences between proton and photon detectors was then generated for both the 175° and 155° detectors. Such a two-dimensional plot for the 155° detector is shown in Fig. 1. The horizontal axis of Fig. 1 represents the proton energy and the vertical axis that of the photon. Each dot on the plot is a coincident event. This plot covers the entire kinematic region, limited only by noise cutoffs at the lower end of both the proton and photon detectors. The p ^{12}Cγ kinematic line, which starts at the energy of the elastic scattered protons, is shown in the figure as the solid line. Because the undetected carbon recoil energy changes slightly with bremsstrahlung photon energy, the kinematic line is not exactly straight and the finite resolutions of detectors make the kinematic line a band, along which the p ^{12}Cγ bremsstrahlung events, including the clusters at photon energies 0.39 and 1.55 MeV, can be easily seen. The biggest cluster is identified to be the ^{23}Na+p inelastic scattering events from the contamination of sodium in the target, which we estimate to be about 1%. The ^{23}Na+p inelastic scattering has a characteristic photon energy of 0.44 MeV and serves as an independent check of the system energy calibrations. The Compton tail from the 0.44-MeV γ rays also interferes with the p ^{12}Cγ kinematic line at photon energies below 0.2 MeV. The energy resolution of the photon detector ranges from 20 keV (FWHM) at 75 keV to 110 keV at 1332 keV.

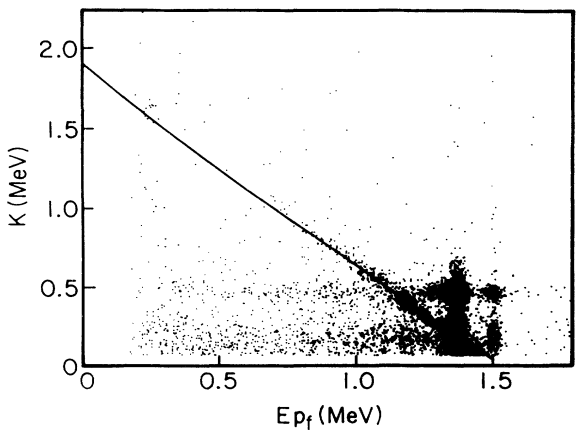

FIG. 1. Coincident events between the final-state protons and photons at an incident proton energy of 2.135 MeV. Each dot corresponds to a coincident event. The p ^{12}Cγ kinematic line is shown as the solid line. Two clusters of points on the kinematic line represent the structures in the bremsstrahlung cross sections at 0.39 and 1.55 MeV. The huge cluster at bottom right is from ^{23}Na+p inelastic scattering.

To get the bremsstrahlung cross section, we project onto the proton axis those events in the kinematic band between the noise and the ^{23}Na interference region. The background from accidental coincidences is very small and contains no structures. The final bremsstrahlung cross section is normalized to the corresponding p ^{12}C elastic scattering cross section. The major correction to the relative cross section comes from the photon detector efficiency. The NaI efficiency is obtained from standard references, such as that of Marion and Young [13] and varies from about 3% at 2 MeV to 10% at 0.5 MeV. The attenuation of photons by detector housing, windows, etc. is estimated to be less than 10%. A nominal uncertainty in those corrections has been added in quadrature to the statistical error to form the final error bars on the data points.

III. THEORY

We consider the p ^{12}Cγ process

$$p(p_i^\mu)+{}^{12}\mathrm{C}(q_i^\mu)\rightarrow p(p_f^\mu)+{}^{12}\mathrm{C}(q_f^\mu)+\gamma(K^\mu)\ , \tag{1}$$

where p_i^μ (p_f^μ) and q_i^μ (q_f^μ) are initial (final) four-momenta of proton and carbon, respectively, and K^μ is the four-momentum of the emitted photon. When K approaches zero, the p ^{12}Cγ process reduces to the corresponding p ^{12}C elastic scattering process

$$p(p_i^\mu)+{}^{12}\mathrm{C}(q_i^\mu)\rightarrow p(\bar{p}_f^\mu)+{}^{12}\mathrm{C}(\bar{q}_f^\mu)\ , \tag{2}$$

where

$$\bar{p}_f^\mu=\lim_{K\rightarrow 0} p_f^\mu$$

and

$$\bar{q}_f^\mu=\lim_{K\rightarrow 0} q_f^\mu\ .$$

The elastic (on-shell) T matrix for the p ^{12}Cγ process may be written as a function of two Lorentz invariants s and t, $T(s,t)$. Here, s is the total energy squared and t is the momentum transfer squared,

$$s=(q_i+p_i)^2=(\bar{q}_f+\bar{p}_f)^2$$

and

$$t=(\bar{p}_f-p_i)^2=(\bar{q}_f-q_i)^2\ . \tag{3}$$

The T matrix may also be written as a function of the incident energy E_i and the scattering angle θ since s and t can be determined from E_i and θ. A nonrelativistic expression for the p ^{12}C elastic scattering amplitude,

$$\bar{u}(\bar{p}_f,\nu_f)T(s,t)u(p_i,\nu_i)\ ,$$

with a set of resonance parameters can be found in a paper by Armstrong *et al.* [14]. This amplitude has been used as an input for all p ^{12}Cγ calculations in the soft-photon approximations.

The bremsstrahlung amplitude M_μ can be written as the sum of the external scattering amplitude M_μ^E and the internal scattering amplitude M_μ^I,

$$M_\mu=M_\mu^E+M_\mu^I\ . \tag{4}$$

Four external emission diagrams which determine M_μ^E are shown in Figs. 2(a)–2(d). In these diagrams, T_a, T_b, T_c, and T_d represent four half-off-shell T matrices which depend upon three Lorentz invariants. In addition to s and t, a half-off-shell T matrix also depends upon the square of the invariant mass, Δ, of the off-mass-shell leg on which the photon emission occurs. Thus, we can define T_x $(x=a,b,c,d)$ as

$$\begin{aligned} T_a &\equiv T(s_i,t_p,\Delta_a)\ , \\ T_b &\equiv T(s_f,t_p,\Delta_b)\ , \\ T_c &\equiv T(s_i,t_q,\Delta_c)\ , \end{aligned} \tag{5}$$

and

$$T_d \equiv T(s_f,t_q,\Delta_d)\ ,$$

where

$$\begin{aligned} &\Delta_a=(q_f+K)^2,\quad \Delta_b=(q_i-K)^2\ , \\ &\Delta_c=(p_f+K)^2,\quad \Delta_d=(p_i-K)^2\ , \\ &s_i=(q_i+p_i)^2,\quad s_f=(q_f+p_f)^2\ , \\ &t_p=(p_f-p_i)^2\ , \end{aligned}$$

and

$$t_q=(q_f-q_i)^2\ .$$

In terms of these four half-off-shell T matrices, M_μ^E can be written as

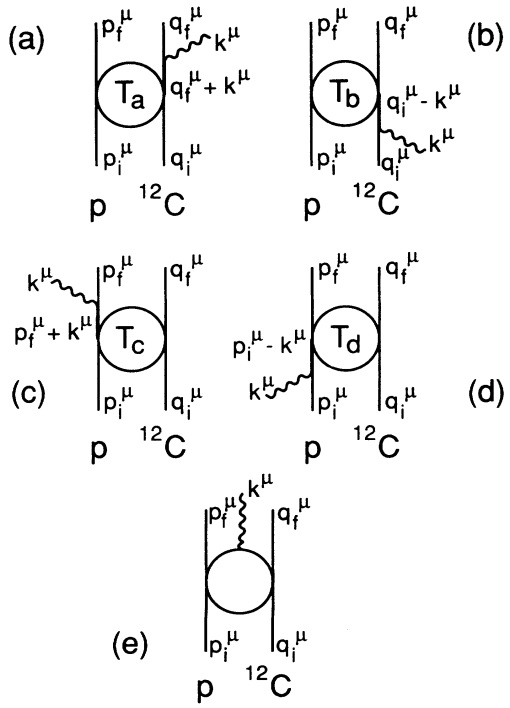

FIG. 2. Feynman diagram for proton-carbon bremsstrahlung: (a)–(d) the external scattering diagrams; (e) the internal scattering diagram.

$$M_\mu^E = Z\frac{q_{f\mu}}{q_f\cdot K}T_a - Z\frac{q_{i\mu}}{q_i\cdot K}T_b + \frac{p_{f\mu}}{p_f\cdot K}T_c - \frac{p_i\mu}{p_i\cdot K}T_d\ , \tag{6}$$

which cannot be calculated if the elastic scattering T matrix is the only input for the calculation. In Eq. (6) $Z=6$ is the atomic number of carbon. Since M_μ^E is not gauge invariant, an internal scattering amplitude M_μ^I is required in order to make the total amplitude gauge invariant. A diagram which represents M_μ^I is shown in Fig. 2(e). In general, the exact expression for M_μ^I is too difficult to obtain. However, Low [10] has shown that the leading term of M_μ^I can be obtained from the gauge-invariant condition

$$M_\mu K^\mu = (M_\mu^E + M_\mu^I)K^\mu = 0 \tag{7a}$$

or

$$M_\mu^I K^\mu = -M_\mu^E K^\mu\ . \tag{7b}$$

To obtain the leading term of M_μ^I from Eq. (7b), M_μ^E must be expanded in powers of K. Such expansion is not unique because T_x $(x=a,b,c,d)$ can be expanded, in general, about $(S_{\alpha_x\beta_x}, t_{\alpha'_x\beta'_x})$, where

$$\begin{aligned} s_{\alpha_x\beta_x} &= \frac{\alpha_x s_i+\beta_x s_f}{\alpha_x+\beta_x}\ , \\ t_{\alpha'_x\beta'_x} &= \frac{\alpha'_x t_p+\beta'_x t_q}{\alpha'_x+\beta'_x}\ , \end{aligned} \tag{8}$$

and $\alpha_x, \beta_x, \alpha'_x$, and β'_x $(x=a,b,c,d)$ are any arbitrary real numbers [1]. Once the leading term of M_μ^I is obtained from Eq. (7), we can combine M_μ^E and M_μ^I to obtain the total amplitude M_μ which can be written in the form

$$M_\mu = \frac{A_\mu}{K} + B_\mu + C_\mu K + \cdots\ . \tag{9}$$

As shown in Ref. [1], A_μ depends only on the elastic T matrix evaluated at $s_{\alpha_x\beta_x}$ and $t_{\alpha'_x\beta'_x}$, while B_μ depends on the derivatives of the elastic T matrix with respect to $s_{\alpha_x\beta_x}$ and $t_{\alpha'_x\beta'_x}$. Moreover, since A_μ and B_μ are independent of the off-shell derivatives [i.e., the derivatives of T with respect to Δ_x $(x=a,b,c,d)$], only the first two terms of the expansion given by Eq. (9) can be evaluated in terms of the p ^{12}C elastic scattering T matrix. Thus, all bremsstrahlung amplitudes in soft-photon approximations (SPA) have the following expression:

$$M_\mu^{\rm SPA} = \frac{A_\mu}{K} + B_\mu\ . \tag{10}$$

Depending upon the choice of parameters, $\alpha_x, \beta_x, \alpha'_x$, and β'_x, these soft-photon approximations can be divided into many different classes [1]. Three classes will be discussed here.

(a) One-energy–one-angle (OEOA) approximation. The most general amplitude in this approximation has the form

$$M_{\mu}^{\mathrm{OEOA}}(s_{\alpha\beta},t_{\alpha'\beta'})=\frac{A_{\mu}^{\mathrm{OEOA}}(s_{\alpha\beta},t_{\alpha'\beta'})}{K}+B_{\mu}^{\mathrm{OEOA}}(s_{\alpha\beta},t_{\alpha'\beta'}) . \quad (11)$$

Here, the leading term, $A_{\mu}^{\mathrm{OEOA}}/K$, depends on the elastic scattering T matrix evaluated at

$$s_{\alpha\beta}=\frac{\alpha s_i+\beta s_f}{\alpha+\beta} \quad (12a)$$

and

$$t_{\alpha'\beta'}=\frac{\alpha' t_p+\beta' t_q}{\alpha'+\beta'} , \quad (12b)$$

and the second term, B_{μ}^{OEOA}, depends on $\partial T/\partial s_{\alpha\beta}$ and $\partial T/\partial t_{\alpha'\beta'}$. Since it is impossible to find a set of $(\alpha,\beta,\alpha',\beta')$ such that B_{μ}^{OEOA} vanishes, M_{μ}^{OEOA} must involve $\partial T/\partial s_{\alpha\beta}$ and $\partial T/\partial t_{\alpha'\beta'}$ in this approximation. In this work, we are mainly interested in how the predicted resonant structure depends on the parameters α and β, so we have used a fixed momentum transfer squared, $t\equiv\lim_{K\to 0}t_{\alpha'\beta'}$ [which is independent of α' and β', see Eq. (3)], in all calculations. In the vicinity of a resonance, either the 1.7-MeV resonance or the 0.5-MeV resonance, the bremsstrahlung spectrum calculated with M_{μ}^{OEOA} will predict a huge resonant peak (mainly due to the B_{μ}^{OEOA} term which involves $\partial T/\partial s_{\alpha\beta}$ although A_{μ}^{OEOA} alone also gives a large resonant peak). If $s_{\alpha\beta}\neq s_i$ (no resonant peak will be predicted if $s_{\alpha\beta}=s_i$), the peak will appear around the photon energy K_{γ} which can be calculated, within 10% error, by the following formula [1]:

$$K_{\gamma}=\left[\frac{\alpha+\beta}{\beta}\right](E_i-E_R)N, \quad \beta\neq 0 , \quad (13)$$

where $N\cong 1$, E_i is the incident proton energy and E_R is the resonant energy. In addition to the position of the resonant structure, the width of the resonant peak, Γ_{γ}, can be predicted by the following formula:

$$\Gamma_{\gamma}=\left[\frac{\alpha+\beta}{\beta}\right]\Gamma_{\mathrm{el}}N , \quad (14)$$

where Γ_{el} is the width of the resonant peak observed in the p ^{12}C elastic scattering cross sections. In Low's approximation, for instance, we choose $\alpha=\beta=1$ and hence the elastic T matrix is evaluated at $\bar{s}=(s_i+s_f)/2$. In this case, the predicted resonant structure will be centered at $K_{\gamma}\cong 2(E_i-E_R)$ and the width of the resonance will be $\Gamma_{\gamma}\cong 2\Gamma_{\mathrm{el}}$.

(b) Two-energy–one-angle (TEOA) approximation. This approximation is a generalization of the original Feshbach-Yennie approximation. A class of amplitude in this approximation can be written as

$$M_{\mu}^{\mathrm{TEOA}}(s_{\alpha_1\beta_1},s_{\alpha_2\beta_2};t)=\frac{A_{\mu}^{\mathrm{TEOA}}(s_{\alpha_1\beta_1},s_{\alpha_2\beta_2};t)}{K}+B_{\mu}^{\mathrm{TEOA}}(s_{\alpha_1\beta_1},s_{\alpha_2\beta_2};t) . \quad (15)$$

The leading term in Eq. (15), $A_{\mu}^{\mathrm{TEOA}}/K$, depends on a T matrix evaluated at $(s_{\alpha_1\beta_1},t)$, and a T matrix evaluated at $(s_{\alpha_2\beta_2},t)$, and the second term, B_{μ}^{TEOA}, depends on $\partial T/\partial s_{\alpha_1\beta_1}$, $\partial T/\partial s_{\alpha_2\beta_2}$, and $\partial T/\partial t$. Here

$$s_{\alpha_n\beta_n}=\frac{\alpha_n s_i+\beta_n s_f}{\alpha_n+\beta_n}, n=1,2 \quad (16)$$

and

$$t\equiv\lim_{K\to 0}t_{\alpha'\beta'}$$

is given by Eq. (3). By varying $\alpha_1,\beta_1,\alpha_2$, and β_2, the amplitudes given by Eq. (15) predict various spectra with one or two resonant peaks (or structures) depending on the values of $s_{\alpha_1\beta_1}$ and $s_{\alpha_2\beta_2}$.

(i) If $s_{\alpha_1\beta_1}\neq s_i\neq s_{\alpha_2\beta_2}$, and $s_{\alpha_1\beta_1}\neq s_{\alpha_2\beta_2}$ (i.e., $\beta_1\neq 0,\beta_2\neq 0$, and $\beta_1\neq\beta_2$), then B_{μ}^{TEOA} in Eq. (15) will depend on $\partial T/\partial s_{\alpha_1\beta_1}$, $\partial T/\partial s_{\alpha_2\beta_2}$, and $\partial T/\partial t$, and the calculated bremsstrahlung spectrum will show double resonant peaks for each p ^{12}C elastic scattering resonance. (That is, two peaks for the 1.7-MeV resonance and another two peaks for the 0.5-MeV resonance.) Applying Eqs. (13) and (14) to this case, we have

$$K_{\gamma}^{(n)}=\left[\frac{\alpha_n+\beta_n}{\beta_n}\right](E_i-E_R)N, \quad n=1,2, \quad (17a)$$

and

$$\Gamma_{\gamma}^{(n)}=\left[\frac{\alpha_n+\beta_n}{\beta_n}\right]\Gamma_{\mathrm{el}}N . \quad (17b)$$

(ii) If $s_{\alpha_1\beta_1}=s_i$ and $s_{\alpha_2\beta_2}\neq s_i$ (i.e., $\beta_1=0$ and $\beta_2\neq 0$), then B_{μ}^{TEOA} in Eq. (15) will depend on $\partial T/\partial s_{\alpha_2\beta_2}$ and $\partial T/\partial t$, and the calculated bremsstrahlung spectrum will have only one (single) resonant peak for each p ^{12}C elastic scattering resonance. The peak will appear at

$$K_{\gamma}^{(2)}=\left[\frac{\alpha_2+\beta_2}{\beta_2}\right](E_i-E_R)N , \quad (18a)$$

and the width will be

$$\Gamma_{\gamma}^{(2)}=\left[\frac{\alpha_2+\beta_2}{\beta_2}\right]\Gamma_{\mathrm{el}}N . \quad (18b)$$

The most interesting example of this approximation is the Feshbach-Yennie approximation, which corresponds to $\alpha_1=\beta_2=1$ and $\beta_1=\alpha_2=0$. The Feshbach-Yennie amplitude (FYA) predicts bremsstrahlung spectrum with single resonant peak for each p ^{12}C scattering resonance at the photon energy $K_{\gamma}^{\mathrm{FYA}}\cong K_0=E_i-E_R$. The width of the peak is $\Gamma_{\gamma}^{\mathrm{FYA}}\simeq\Gamma_{\mathrm{el}}$.

(c) Two-energy–two-angle (TETA) approximation. We shall discuss only a special TETA approximation (TETAS) here. The amplitude for this TETAS has the form [9]

$$M_{\mu}^{\mathrm{TETAS}}(s_i,s_f;t_p,t_q)=\frac{A_{\mu}^{\mathrm{TETAS}}(s_i,s_f;t_p,t_q)}{K}+B_{\mu}^{\mathrm{TETAS}}(s_i,s_f;t_p,t_q) , \quad (19a)$$

where

$$\frac{A_\mu^{\text{TETAS}}}{K}=Z\left[\frac{q_{f\mu}}{q_f\cdot K}-\frac{(q_f+p_f)_\mu}{(q_f+p_f)\cdot K}\right]T(s_i,t_p)$$
$$-ZT(s_f,t_p)\left[\frac{q_{i\mu}}{q_i\cdot K}-\frac{(q_i+p_i)_\mu}{(q_i+p_i)\cdot K}\right]$$
$$+\left[\frac{p_{f\mu}}{p_f\cdot K}-\frac{(q_f+p_f)_\mu}{(q_f+p_f)\cdot K}\right]T(s_i,t_q)$$
$$-T(s_f,t_q)\left[\frac{p_{i\mu}}{p_i\cdot K}-\frac{(q_i+p_i)_\mu}{(q_i+p_i)\cdot K}\right] \quad (19b)$$

and

$$B_\mu^{\text{TETAS}}=0\ . \quad (19c)$$

The most interesting features of this amplitude are as follows. (i) The second term in each of the square brackets in Eq. (19b) [i.e., the term involving $(q_i+p_i)_\mu/(q_i+p_i)\cdot K$ or $(q_f+p_f)_\mu/(q_f+p_f)\cdot K$] is called the gauge term since it is required to make the total amplitude gauge invariant. As shown in Ref. [9], these gauge terms represent photon emissions from the charge of the intermediate particle ^{13}N*. (ii) M_μ^{TETAS} is free of any derivative of T matrix with respect to s or t. This makes TETAS a good approximation for bremsstrahlung processes in the energy region of a resonance. In fact, a recent study shows that all the available p ^{12}Cγ data (and most of the $\pi^{\pm}p\gamma$ data) can be described by this TETAS approximation [9]. (iii) The amplitude M_μ^{TETAS} depends on T matrix evaluated at four different sets of (s,t):(s_i,t_p),(s_i,t_q),(s_f,t_p), and (s_f,t_q). That is, M_μ^{TETAS} does not depend on any combination of s_i and s_f. This means that the TETAS approximation will predict a bremsstrahlung spectrum with a single resonant peak for each p ^{12}C elastic scattering resonance. The peak will appear at $K_\mu^{\text{TETAS}}\cong K_0$ and its width will be $\Gamma_\mu^{\text{TETAS}}\cong\Gamma_{\text{el}}$.

It is clear that different approximations predict different spectra. More precisely, the predicted resonant structure will be quite different for different approximations. Thus a precise measurement of the resonant structure (its position and width) can provide a very sensitive test of various approximations.

IV. RESULTS, DISCUSSION, AND CONCLUSION

The results of our measurements are shown in Figs. 3 and 4. In these figures, the ratio of the p ^{12}Cγ cross section to the p ^{12}C elastic scattering cross section,

$$\frac{d^3\sigma_\gamma}{d\Omega_p d\Omega_\gamma dK}\Big/\frac{d\sigma_{\text{el}}}{d\Omega_p}\ , \quad (20)$$

is plotted as a function of K at an incident proton energy of 2.135 MeV for two scattering angles: one at 155° and another one at 175°. We have extended the range of measurements up to 1.7 MeV in photon energy in order to search for all possible resonant structures. Each measured bremsstrahlung spectrum exhibits one resonant peak at $K_\gamma=0.39$ MeV and suggests another peak at $K_\gamma=1.55$ MeV. In the subsequent discussion, we will refer to both of these peaks with the understanding that the experimental evidence for the existence of the 1.55-MeV peak is weaker than that for the 0.39-MeV peak. The 0.39-MeV peak is identified to be the structure due to the 1.7-MeV elastic scattering resonance while the 1.55-MeV peak is identified to be the strucutre due to the 0.5-MeV elastic scattering resonance. No other resonant structure has been found in the entire photon energy region. These measured spectra are compared with the theoretical predictions calculated in the OEOA approximation, the TEOA approximation and the TETAS approximation. The results and implications of the comparison can be summarized as follows.

(i) The observed peaks at $K_\gamma=0.39$ and 1.55 MeV cannot be described by any OEOA approximation with the elastic T matrix evaluated at $s_{\alpha\beta}$ (i.e., any linear combination of s_i and s_f). The first peak predicted by this approximation will appear at, using Eq. (13),

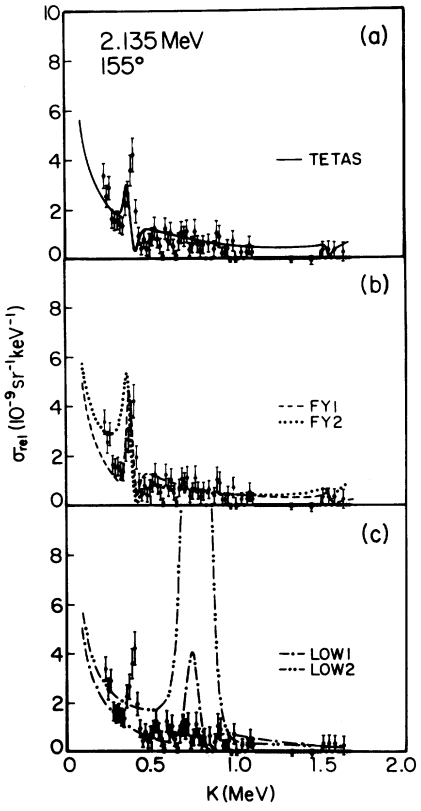

FIG. 3. The p ^{12}Cγ cross section relative to the p ^{12}C elastic scattering cross section as a function of photon energy at an incident proton energy of 2.135 MeV for the scattering angle of 155°. The experimental data are compared with the theoretical predictions calculated in (a) the TETAS approximation using Eq. (19), (b) the Feshbach-Yennie approximation, Eq. (25) (for the dashed curve, FY1) and Eq. (26) (for the dotted curve, FY2), and (c) Low's approximation using Eq. (23) (for the dash-dotted curve, LOW1) and Eq. (24) (for the dash-double-dotted curve, LOW2).

$$K_\gamma = \left[\frac{\alpha+\beta}{\beta}\right](E_i - E_R)N ,$$

$$= \left[\frac{\alpha+\beta}{\beta}\right](2.135-1.734)\left[\frac{12}{13}\right] \text{ MeV}$$

$$= 0.37\left[\frac{\alpha+\beta}{\beta}\right] \text{MeV} , \quad (21)$$

$\beta \neq 0$, and the second peak at

$$K_\gamma = \left[\frac{\alpha+\beta}{\beta}\right](2.135-0.461)\left[\frac{12}{13}\right] \text{ MeV}$$

$$= 1.55\left[\frac{\alpha+\beta}{\beta}\right] \text{ MeV} , \quad (22)$$

rather than at $K_\gamma = 0.39$ and 1.55 MeV, respectively, as observed in this experiment. For example, if we choose $\alpha=\beta=1$ and evaluate the elastic T matrix at $s_{11}=(s_i+s_f)/2$, then the first peak will be predicted at 0.74 MeV in the bremsstrahlung spectrum; the second peak, at 3.1 MeV, is kinematically impossible. As shown in Figs. 3(c) and 4(c), our exact calculation using the OEOA amplitude confirms this prediction. In these figures, LOW1 represents the calculation using the leading term of Eq. (11) with $\alpha=\beta=1$ and $t_{\alpha'\beta'}=t$,

$$M_\mu^{\text{LOW1}}(s_{11},t) = \frac{A_\mu^{\text{OEOA}}(s_{11},t)}{K} , \quad (23)$$

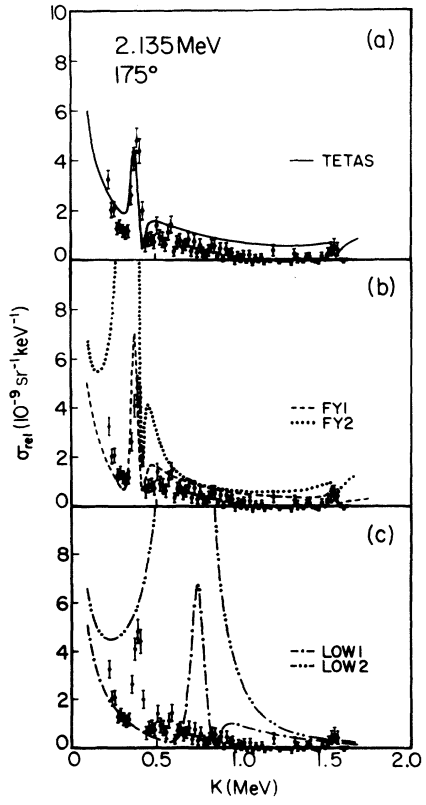

FIG. 4. Same as Fig. 3, but for 175°.

and LOW2 represents the calculation using the complete amplitude given by Eq. (11) with $\alpha=\beta=1$ and $t_{\alpha'\beta'}=t$,

$$M_\mu^{\text{LOW2}}(s_{11},t) = \frac{A_\mu^{\text{OEOA}}(s_{11},t)}{K} + B_\mu^{\text{OEOA}}(s_{11},t) . \quad (24)$$

The giant peak (predicted by the LOW2 approximation at 0.74 MeV) comes from the B_μ^{OEOA} term which involves $\partial T/\partial s_{11}$. It is true that if we choose $\alpha=0$ or $\beta \gg \alpha$, then $(\alpha+\beta)/\beta \to 1$ and two peaks will be predicted at 0.37 and 1.55 MeV in the bremsstrahlung spectrum. However, the width and shape of these predicted giant peaks disagree drastically with the width and shape of the small peaks observed experimentally. This fact has already been pointed out in Ref. 1.

(ii) As shown in Figs. 3(b) and 4(b), the positions (in photon energies) of two observed resonant peaks can be correctly predicted by the Feshbach-Yennie approximation even though the width and height of the 0.37-MeV peak disagree with the data for the 175° case. The Feshbach-Yennie amplitude depends on one elastic T matrix evaluated at s_i and $t, T(s_i,t)$, and another elastic T matrix evaluated at s_f and t, $T(s_f,t)$. In Figs. 3(b) and 4(b), FY1 represents the calculation using the leading (principal) term of Eq. (15) with $\alpha_1=\beta_2=1$ and $\beta_1=\alpha_2=0$,

$$M_\mu^{\text{FY1}}(s_i,s_f;t) = \frac{A_\mu^{\text{TEOA}}(s_i,s_f;t)}{K} , \quad (25)$$

and FY2 represents the calculation using the complete amplitude given by Eq. (15) with $\alpha_1=\beta_2=1$ and $\beta_1=\alpha_2=0$,

$$M_\mu^{\text{FY2}}(s_i,s_f;t) = \frac{A_\mu^{\text{TEOA}}(s_i,s_f;t)}{K} + B_\mu^{\text{TEOA}}(s_i,s_f;t) . \quad (26)$$

For both the 155° and 175° cases, the agreement with the data is better only if the amplitude M_μ^{FY1} is used in the calculation. This implies that the B_μ^{TEOA} term which depends on $\partial T/\partial t$ may give poor results in the energy region of a resonance for some cases. Our study also shows that other TEOA amplitudes which depend on any linear combination of s_i and s_f cannot be used to describe the resonant peaks observed experimentally. Reasons are as follows. [For details, see the discussion given in (b) of Sec. III.] Since only one single peak in bremsstrahlung spectrum has been experimentally observed for each elastic scattering resonance (i.e., double peaks do not exist), the TEOA amplitude which could be used to describe the data should depend on an elastic T matrix evaluated at s_i and $t, T(s_i,t)$. Furthermore, from the position and width of the observed peaks, we can conclude that the amplitude must also depend on another elastic T matrix evaluated at s_f and t, $T(s_f,t)$. To understand the last point, let us use the 0.39-MeV peak as an example. If we take K_γ to be 0.39 MeV from the experiment, then Eq. (18a) gives

$$0.39 = 0.37\left[\frac{\alpha_2+\beta_2}{\beta_2}\right] , \quad (27)$$

since $(E_i - E_R)N = 0.37$ MeV [see Eq. (21)]. Solving Eq. (27), we find

$$\frac{\alpha_2}{\beta_2} \cong 0.05 , \tag{28}$$

which is consistent with $\alpha_2/\beta_2 = 0$ or $\alpha_2 = 0$ and $\beta_2 \neq 0$. Remember that Eq. (18a) is only a good approximation for finding the value of K_γ, it is not an exact formula. If we use $\alpha_2/\beta_2 = 0.05$ in a TEOA amplitude, then the amplitude which depends on $\partial T/\partial s_{\alpha_2\beta_2}$ would give much higher peaks with wider widths, in disagreement with experiment. On the other hand, if we choose $\alpha_2/\beta_2 = 0$, then the amplitude would be independent of $\partial T/\partial s_{\alpha_2\beta_2}$ and a smaller peak, which is in better agreement with the observed one, would be predicted by the amplitude. This implies that we should choose $\alpha_2 = 0$ and $\beta_2 \neq 0$. In other words, the Feshbach-Yennie amplitude is the best amplitude in the TEOA approximation.

(iii) The spectra calculated in the TETAS approximation [using the TETAS amplitude given by Eq. (19)] are shown in Figs. 3(a) and 4(a). From these figures, we can find that the positions of two observed resonant peaks can be described by the TETAS amplitude [i.e., the amplitude M_μ^{TETAS} given by Eq. (19a)] and the spectra predicted by this amplitude are in much better agreement with the data than those spectra predicted by other amplitudes. Although the amplitude M_μ^{FY1} defined by Eq. (25) is also a good approximation, as we have already discussed in (ii), there is a substantial difference between M_μ^{TETAS} and M_μ^{FY1}. The amplitude M_μ^{FY1} belongs to the TEOA approximation. It is the leading term of Eq. (15) with $\alpha_1 = \beta_2 = 1$ and $\beta_1 = \alpha_2 = 0$. Since the second term, B_μ^{TEOA}, does not vanish in general, the amplitude M_μ^{FY1} has ignored an important contribution from this second term without justification. In fact, a large contribution from the B_μ^{TEOA} term is found in the 175° case. This can be seen from Fig. 4 if we examine the difference between the spectra predicted by the amplitude M_μ^{FY1} and the spectrum predicted by the amplitude M_μ^{FY2} [Eq. (26)]. The amplitude M_μ^{TETAS}, on the other hand, does include the B_μ^{TETAS} term, the second term, but its contribution is identically zero. It should be emphasized that the good agreement between the experimental data and the theoretical predictions calculated with the amplitude M_μ^{TETAS} and M_μ^{FY1} supports the argument that the best amplitude for a bremsstrahlung process in the energy region of a resonance is the amplitude which is free of terms involving $\partial T/\partial s$ and $\partial T/\partial t$ [9].

In conclusion, we have measured the $p\ ^{12}C\gamma$ cross sections as a function of K at 2.135 MeV for the scattering angles of 155° and 175°. By extending the range of photon energy up to 1.7 MeV, which is near the maximum photon energy, we have found two resonant peaks at 0.39 and 1.55 MeV. These peaks are identified as due to the elastic $p\ ^{12}C$ scattering resonances at 1.7 and 0.5 MeV, respectively. These measured cross sections with two resonant peaks have been used to test various soft-photon approximations, including the OEOA approximation, the TEOA approximation, and the TETAS approximation. The result of our test shows that the data can only be described by the two-energy approximation which depends on s_i and s_f separately but not on any linear combination of s_i and s_f. The best two-energy approximation is found to be the TETAS approximation which is free of any derivative of the elastic scattering T matrix with respect to s or t.

ACKNOWLEDGMENTS

We wish to thank T. Lubicich for maintaining reliable operation of the Dynamitron Accelerator. The CUNY University Computer Center is acknowledged for providing computer resources for the theoretical calculations. This work was supported in part by a grant from the Professional Staff Congress–Board of Higher Education Faculty Research Award Program of CUNY.

[1] M. K. Liou and Z. M. Ding, Phys. Rev. C **35**, 651 (1987).
[2] C. Maroni, I. Massa, and G. Vannini, Nucl. Phys. **A273**, 429 (1976); A. Cristallini, C. Maroni, I. Massa, and G. Vannini, Phys. Lett. **56B**, 245 (1975).
[3] C. C. Trail, P. M. S. Lesser, A. H. Bond, M. K. Liou, and C. K. Liu, Phys. Rev. C **21**, 2131 (1980).
[4] H. Taketani, M. Adachi, N. Endo, and T. Suzuki, Phys. Lett. **113B**, 11 (1982); H. Taketani, N. Endo, G. Ishikawa, T. Suzuki, M. Adachi, T. Kohno, A. Makishima, and T. Ikuta, Nucl. Instrum. Methods **196**, 283 (1982).
[5] P. M. S. Lesser, C. C. Trial, C. C. Perng, and M. K. Liou, Phys. Rev. Lett. **48**, 308 (1982).
[6] M. K. Liou, C. K. Liu, P.M.S. Lesser, and C. C. Trail, Phys. Rev. C **21**, 518 (1980).
[7] C. C. Perng, G. J. Jan, and M. K. Liou, Phys. Rev. C **23** 2357 (1981); G. J. Jan, C. C. Perng, and M. K. Liou, Phys. Lett. **85B**, 25 (1979).
[8] C. K. Liu, M. K. Liou C. C Trail, and P. M. S. Lesser, Phys. Rev. C **26**, 723 (1982).
[9] Z. M. Ding and M. K. Liou, Mod. Phys. Lett. A **3**, 1065 (1988); Z. M. Ding, Dahang Lin, and M. K. Liou, Phys. Rev. C **40**, 1291 (1989).
[10] F. E. Low, Phys. Rev. **110**, 974 (1958).
[11] H. Feshbach, and D. R. Yennie, Nucl. Phys. **37** 150 (1962).
[12] C. C. Perng, D. Yan, P. M. S. Lesser, C. C. Trail, and M. K. Liou, Phys. Rev. C **38**, 514 (1988).
[13] J. B. Marion and F. C. Young, *Nuclear Reaction Analysis: Graphs and Tables* (North-Holland, Amsterdam, 1968).
[14] J. C. Armstrong, M. J. Baggett, W. R. Harris, and V. A. Latonne, Phys. Rev. **144**, 823 (1966).